Parametric study of geometry optimization for corrugated tubes for maximization of heat transfer of internal flows

André Cacilhas Machado
andrecacilhasmachado@tecnico.ulisboa.pt

Instituto Superior Técnico, Universidade de Lisboa, Portugal

January 2021

Abstract

This work addressed the influence of the geometry of corrugated tubes, namely the corrugated pitch and depth, in the head losses and in the heat transfer, for a range of Reynolds numbers from 200 to 6000. Distilled water was the working fluid, and a constant heat flux was imposed on the tubes. A numeric work was also performed using the $k-\omega$ SST turbulence model. The numerical model was validated with the obtained experimental data. The corrugated tubes have a greater thermal performance for a Reynolds number in the transition flow regime ($1000 < Re_d < 2000$) when compared with the smooth tube with, a maximum value of 4,7 obtained numerically. The critical Reynolds number for this work seems to be only a function of the dimensionless corrugated depth and not the dimensionless pitch. The tubes have a friction coefficient gradient very similar to the effects of the roughness in smooth tubes, as observed in the Moody diagram. The heat transfer is augmented with corrugation depth but decreases with the corrugation pitch. The head losses increase as the corrugation depth increases and the inverse trend is observed with the pitch. The dimensionless depth causes a small increase ($0 < |\Delta Nu| \lesssim 3{,}4$) in the Nusselt number when compared with the dimensionless pitch ($0 < |\Delta Nu| \lesssim 8{,}8$). Any significant heat transfer increase is observed as the flow regime passes from turbulent to laminar regime, for corrugated tubes in fully developed flow. The laminar regime only showed an increase in heat exchange only when the flow is not fully developed.

Keywords: Internal Flow, Heat Transfer Enhancement, Transition from laminar to turbulent regime, Turbulent Regime, Corrugated Tubes, CFD.

1. Introduction

The study and the search of equipment and other forms to augment the efficiency of systems have drawn more attention in recent times. One of the most important devices in the electrical and automotive industry is the compact heat exchangers. In addition to occupying a smaller volume, they also have superior thermal efficiencies due to the shape and geometry of the pipes used for this purpose.

Corrugated tubes have been widely used to increase heat exchange in systems, but it is now necessary to perform an optimization study of their own geometry to be able to identify parameters that can improve thermal energy transport and possibly reduce pressure losses. It is a simple, inexpensive, and effective technique that can be produced with ease. Kareem *et al.* [1] has done a review in literature in many articles presented over the years for the corrugated tubes. In a previous work, the experimental and numerical characterization of the effect of corrugation on the flow inside metal tubes was carried out, used specifically in models of compact exchangers that are being developed for the automotive industry. Following the previous work, it is now intended to carry out the parametric study of optimization of the geometry of the corrugation, namely the pitch, depth, and inclination of the corrugation, which maximizes the dissipated calorific power, minimizing the pumping power.

1.1. Objectives

This work aims to study the effect of changing corrugation parameters since the corrugation itself increases heat transmission. It is intended to describe the effect of changing the pitch of the helices (p) and the depth (e) in the head losses and in the heat transfer.

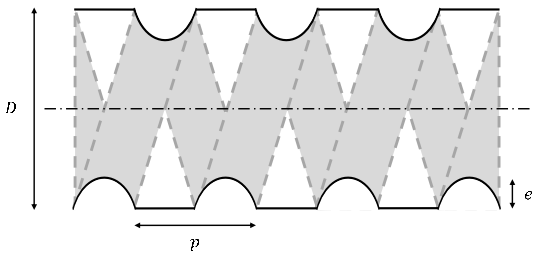

Figure 1 – Geometric parameters of a tube with spiral corrugation.

It is also intended to verify which geometry allows to obtain the best performance against the various regimes of the flow. For this, a constant heat flux is imposed on the walls of the pipe through electric current by Joule effect. The experimental component will serve as validation of the numerical model, which is relevant in the more detailed inference of this exercise of characterization of the effect of geometry on the efficiency of the pipes in terms of head loss and heat transfer.

1.2. Corrugated tubes

As mentioned before, the corrugated tubes are one of low-cost method to improve the efficiency of heat transfer between fluids. García *et al*. [2] refer that artificial rugosity has a greater effect on head losses than in heat transfer. They also state that the geometry has a great impact on the transition from laminar to turbulent flow and on the type of transition: smooth or sudden. For Reynolds number values greater than 2000, the corrugated and tubes with dimples are more advantageous than other strategies. Andrade *et al*. [3] mention that the existence of these spiral corrugations inside the flow will induce a secondary movement also in a spiral. In a recent study, Cruz [4] developed an experimental and numerical work to describe the flow pattern generated by the geometry inside the conduit. The increase of the corrugation depth will increase fluid turbulence and augment the mixing of the center fluid with a lower temperature with the higher one located at the wall. This process will improve the heat transfer at the cost of larger head losses when compared with smooth tubes. Vicente *et al*. [5] observed that the transition from the laminar to the turbulent flow regime occurs smoothly without instabilities at a lower Reynolds number (lower than 1300) and the transition is endorsed by the severity index, ϕ, defined by:

$$\phi = \frac{e^2}{pd} \tag{1.1}$$

These authors also determined that the critical Reynolds number for the transition is only a function of the dimensionless corrugation depth, e/d, and not the dimensionless pitch, p/d. They also present correlations for their results (differences of less than 5% between the correlations and their experimental data) including one for the critical Reynolds number (Re) with an error below 15%.

$$Re_{crit} = 2100\left(1 + 1{,}18 \times 10^7 \left(\frac{e}{d}\right)^{3.8}\right)^{-0{,}1} \tag{1.2}$$

Vicente *et al*. [6], in another study, report the effect of the Prandtl number over the heat transfer, where they observed that the Nusselt number was more influenced in these tubes than in the smooth ones for the used Reynolds number interval. Correlations were presented, and they show that the corrugated depth has a positive effect on the Nusselt number. The pitch has a negative influence on the heat transfer. In an article published by Córcoles-Tendero *et al*. [7], a numerical study was performed using the results from Vicente *et al*. [6] to validate the numerical model. The authors used two meshes, a very fine mesh and a coarser one, with a tridimensional model. The finer mesh presented the lowest errors (using experimental data) when compared to the other one. Another numeric model used by Wang *et al.* [8], where they perform the characterization of the flow as well as study the influence of geometry, show that the intensity of the swirl flow increases as the corrugation depth increases. Values below 0,02 for this parameter (e/d) will cease the swirl. The dimensionless pitch, when reduced, will augment the swirl effect. Wang *et al*. [8] present correlations where these geometric parameters have an influence on the Nusselt number and on the friction factor. The dimensionless pitch (when increased) reduces both heat transfer and friction losses. The dimensionless corrugation depth augments the Nusselt number at the cost of a higher friction factor.

Jin *et al*. [9] have done a parametric study of six corrugated tubes, each with six spiral helices in each section, for high Reynolds number ($10^4 < Re_D < 6 \times 10^4$), with various dimensionless pitch and depth. The authors found the same behavior reported in [6] and [8], providing correlations which demonstrate the geometry effects on both head losses and heat transfer.

Pethkool *et al*. [10] have done a similar study but found that when they increased the dimensionless pitch, both the friction factor and the Nusselt number increased as opposed to the previous research. The dimensionless corrugation depth exhibited the same behavior as in [6], [8] and in [9]. Their Reynolds number range was $5000 \lesssim Re \lesssim 60000$.

Another way to select the best geometry for what regime is by comparing the data obtained with the results from the smooth circular tubes. This can be done by evaluating the thermal performance, η.

$$\eta = \frac{Nu_{co}}{Nu_l} \times \left(\frac{f_l}{f_{co}}\right)^{\frac{1}{3}} \tag{1.3}$$

Where Nu_l and f_l are the Nusselt number and friction factor for the smooth tube and the remaining parameters, Nu_{co} and f_{co}, for the corrugated conduits. For the circular smooth tubes, this performance corresponds to 1 in all regimes. Kareem *et al*. [1] said that many authors used this performance factor (1.3).

In this work, five tubes with different geometries, with their parameters listed in Table I. All the tubes are made of stainless steel AISI 304 with a thermal conductivity of 16,2 W/mK [11]. The parameters are the same as the ones illustrated in Figure 1.

2. Numeric model implementation

2.1. Computational domain

To obtain the domain and geometry in CAD, a cut was made to each of the tubes and then with a microscope, the inner sections of the tubes were removed as can be seen in Figure 2. With the help of the software AUTOCAD 2019 [12], a CAD model was drawn and then the 3D model. All the sections have their geometric parameters described in Table I.

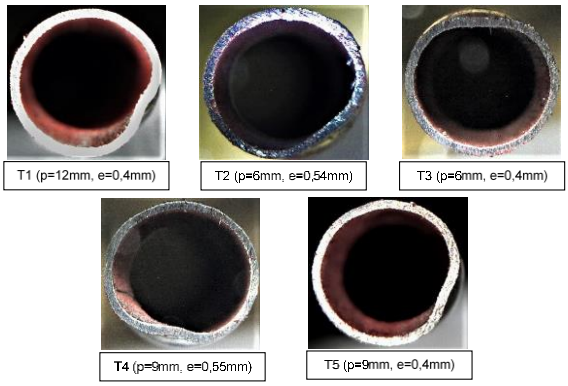

Figure 2 – Tubes sections.

Table I - Geometric parameters of the corrugated tubes.

Tube	d_{ext} [mm]	d_{in} [mm]	p [mm]	e [mm]	ϕ [-]	p/d_{in} [-]	e/d_{in} [-]
T1	5	4,5	12	0,4	0,003	2,67	0,089
T2	5	4,5	6	0,54	0,011	1,33	0,12
T3	5	4,5	6	0,4	0,006	1,33	0,089
T4	5	4,5	9	0,55	0,007	2	0,122
T5	5	4,5	9	0,4	0,004	2	0,089

2.2. STAR-CCM+ 2019

The program used to simulate the tubes used in this work is the Siemens' software STAR-CCM+ 2019 [13]. This CFD program has a huge variety of options for the mesh and many physics models. The mesh used for this problem was a polyhedral one, since it gives a good cell number but also a good solution. Also, this mesh has the possibility to create sections along the tube axis (Generalized cylinder). It was also created a layer close to the walls to capture the viscous effects and heat transfer. Figure 3 and Figure 4 show the type o meshing used for all simulations.

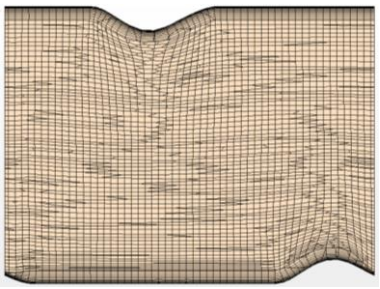

Figure 3 - Example of pitch mesh with longitudinal cut.

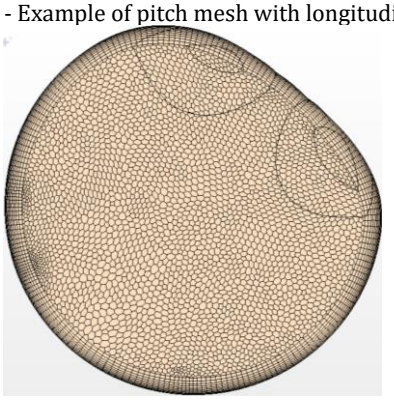

Figure 4 - Example of cross-section mesh.

To model the physics of the problem, assumptions were made such as constant properties and incompressible fluid. There are no buoyancy effects since the temperature's differences were very low. So, the models used in this case are:

- Constant density
- Liquid (water)
- Tridimensional
- Segregated Flow
- Segregated Fluid Temperature
- Steady / Implicit unsteady depending on the regime
- Laminar / Turbulent (Reynolds Average Navier-Stokes Equations) depending on the regime
- $k-\omega$ SST (Menter) Turbulence Model

This program solves the governing equations using the Finite Volume Method [13] and the segregated solver uses the SIMPLE (Semi-Implicit Method Pressure Linked Equations) algorithm in which Deng et. al. [14] explain how it works.

2.3. Verification and Validation

With every numeric work, it is necessary to perform a verification of the model. Sargent [15] describes it as verifying if the program is solving the equations right. It was monitored both the desired quantities and the residuals assuring they went bellow by at least 10^{-4}. Also, for this work, a grid independence study was made to ensure a good solution in a not intensive mesh. Figure 5 shows the convergence study for all tubes at the same Reynolds.

The selected mesh provided a variation below 1% over the friction factor to the next higher cell number mesh. Table II presents the number of cells for each tube depending on the cell base size. The entries marked in green represent the selected meshes for each tube. The validation process consists in verifying if the program is solving the right equations [15].

To validate the results from the simulations, an experimental work, described in in section 4, was performed and the relevant data were obtained that were used to compared with those obtained numerically in section 5.

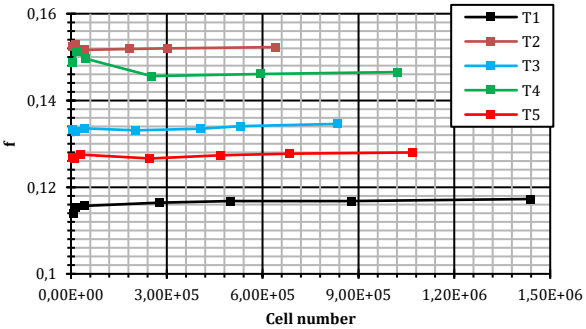

Figure 5 – Mesh convergence study ($Re = 1000$)

Table II - Number of cells depending on the base size for the convergence study

Base size	Cell Number				
[*mm*]	T1	T2	T3	T4	T5
1	*7950*	*5840*	*5580*	*5380*	*5460*
0,5	*16720*	*13473*	*15900*	*18090*	*12390*
0,25	*43920*	*43353*	*42301*	*45478*	*31800*
0,1	*276930*	*182902*	*201635*	*253232*	*247837*
0,075	*499777*	*302989*	*406778*	*595551*	*467028*
0,0625	*877655*	-	*530959*	-	*684318*
0,05	*1437654*	*639705*	*833550*	*1023082*	*1068577*

3. Experimental Work

The test bench was initially developed by Ferreira [16]. Subsequently, the intervention of Nikulin *et al*. [17] and Andrade [18] allowed improvements in the methodology of joining the tubes and in the measurement and data acquisition equipment. In a previous work carried out by Cruz [4], the resulting experimental bench was experimentally validated, both for smooth tubes and corrugated tubes, and compared the results with some correlations presented in the literature, as well as numerical results. Figures 6 and 8 shows the experimental setup used in this thesis.

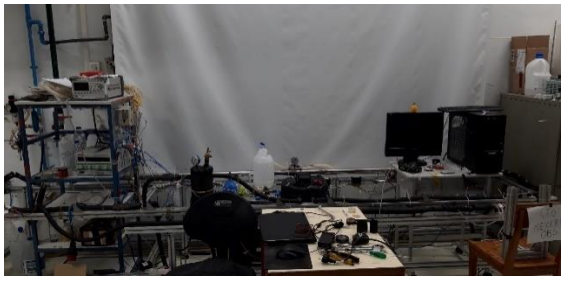

Figure 6 – Testing setup used in this work

This station has an inlet valve (1) where you can fill the reservoir (2) with the test fluid. The electric pump (model GE 5KH36MNA445X) (3) allows to create the mass flows throughout the circuit. Although the pump used in other works had the possibility to change its operating frequency, allowing an easier way to change the mass flow of the circuit, the current one only works with a fixed power. But the presence of valves (4) and (9) allows to adjust the flow rate for the main circuit. Valve (4) is only partially closed when lower flow rates are needed, always leaving it open for higher mass flows ($0 < \dot{m} < 110\ kg/h$). Valve (9) is the most important to change the flow rates because it is inserted in a circuit where the working fluid goes into recirculation to the reservoir (2). The equipment (5), a Cori-FLOW M15 Coriolis flowmeter, measures some important parameters such as the mass flow rate, the entry temperature in the investigation zone (6) and (7) and the mass volume of the fluid it passes through. Part (6) and (7) are the areas of interest for the study to be carried out. After flowing through the corrugated tubes, the working fluid will pass through a coil (8) (cooling unit Embranco model UNT6222GK) that is only operational if it is necessary to reduce the temperature of the fluid to desired values and in case of overheating. Figure 7 represents the entire system circuit.

The tubes are connected by mechanical connections. Copper wires are welded at the ends of the assembly, which are then connected to a power source of electric DC current VOLTEQ HY5050EX that serves to generate heat in the pipes by Joule Effect. The last tube has T-connections so that absolute pressure sensors can be connected by tubes, which subsequently allow to calculate the pressure drop ΔP. In the section of the tube where there is an imposed heat flux, 4 type K thermocouples equally spaced between each other (dimensions and distances shown in Table III and Figure 9) are also installed. Thermocouples were glued with thermal mass and thermal tape to improve the contact and standardize the temperature of each point. These thermocouples, however, are located outside the tube so an estimate of the internal temperature of the tube wall is required.

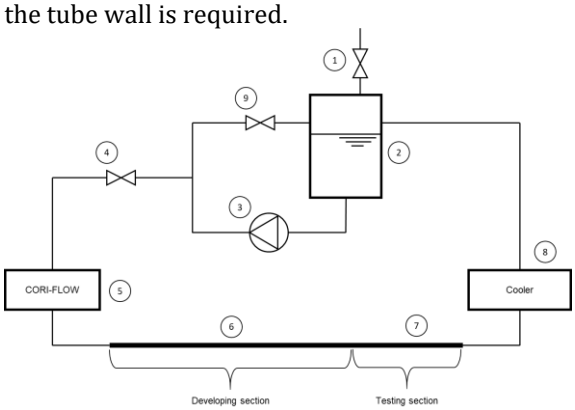

Figure 7 - Schematic representation of the test circuit. 1)Valve, 2) Reservoir, 3) Electric pump model GE 5KH36MNA445X, 4) Valve, 5) Coriolis flowmeter CORI-FLOW M15, 6)Developing section , 7) Testing section, 8)Cooling unit Embranco model UNT6222GK, 9) Valve

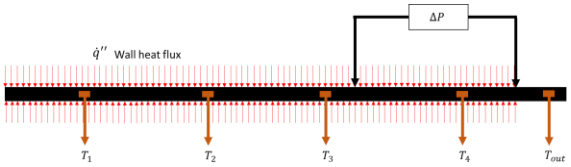

Figure 8 – General scheme of the testing zone, position of thermocouples and absolute pressure sensors.

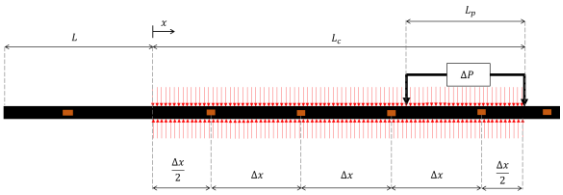

Figure 9 - Sensor positions as well as the size of the corrugated pipe.

The heat power generated by the passage of the electric current is due to the joule effect. But not all the energy released is absorbed by the working fluid and for this reason it cannot be used to calculate the parameters that are intended to be obtained. However due to the presence of three thermocouples, two at the input (T_{in} and $T_{in\,2}$) and one at the outlet (T_{out}) it is possible to estimate the power received by the circulating fluid. It is estimated on average that about 19 to 25.7% of the energy supplied by the electric source VOLTEQ HY5050EX was lost during all tests. The following figure shows the laboratory-mounted scheme. Figure 8 is a schematic representation of the testing zone.

Table III - Parameters and lengths of the assembly of sensors and electrical cables

Tube	L (mm)	L_{con} (mm)	L_p (mm)	Δx (mm)
T1	620	830	285	207,5
T2	550	790	205	197,5
T3	515	830	285	207,5
T4	475	895	240	223,75
T5	510	835	285	207,5

Uncertainties were also evaluated using the guidelines of [19] and [20]. Table *IV* discloses the equipment uncertainties.

Table IV - Uncertainties of instrument measurements.

Parameter	Uncertainty	Unity
Diameter	$\pm$0,05	[mm]
Length	$\pm$5	[mm]
Inlet Temperature	$\pm$0,2	[K]
Thermocouples	$\pm$1	[K]
Density	$\pm$5	[kg/m^3]
Mass flow rate	$\pm$0,2	[%]
Pressure drop	$\pm$1	[%]

4. Results

4.1. Analysis of natural and forced convection

In a previous study, Andrade [18] reported that convection is mostly forced, and the natural one can be neglected when he performed the tests on the bench described in section 4. Andrades's analysis was based on the evaluation of the Richardson number. The Richardson's number:

$$Ri = \frac{g\beta\left(T_{s,+} - T_{ent}\right)D_h}{\overline{u}^2} \qquad (4.1)$$

g being gravitic acceleration (9,81 m/s^2), β the thermal expansion coefficient, $T_{s,+}$ the maximum wall temperature, T_{ent} the temperature of the fluid at the inlet and $\overline{u}$ the average velocity. It was again verified that Richardson number is less than 0.1 for all data points (except for one point in the laminar regime due to low speed). Thus, it is again concluded that this problem is dominated by forced convection and that natural convection is negligible.

4.2. Numeric model Validation

All numeric models were validated using the experimental data. It was not possible to obtain data that fits the numeric models in the laminar regime since the entry thermal length is very high. There was one tube (T5 p=9mm, e=0,4mm) where the temperature difference was lower than the other cases. The Nusselt number is highly dependent of the temperature difference. However, since all models have the same type of geometry it was considered validated, nevertheless.

4.3. Effect of pitch variation (T1 vs. T3 vs. T5)

According to the scientific evidence presented in the theoretical grounds, it is expected that the friction factor, f, has an increase with the decrease of the pitch, p. The data obtained for each tube with the same corrugation depth, $e = 0{,}4\ mm$, confirms this trend in the turbulent regime. However, this trend is not clear in the laminar regime in terms of the experimental data, possibly because there are some errors, and because it is the regime where there is greater uncertainty besides the sensors presenting an absolute pressure difference when the circuit is at rest. It is verified that the larger pitch tube (12 mm) leads to the lowest pressure losses, as predicted. Regarding the other two pitches (p=9mm and p=6mm) this trend is no longer clear. By the numerical work, it is verified that there is an increase in head losses as the pitch decreases (maintaining the corrugation depth constant) both in the laminar regime and in the turbulent regime. In the laminar flow regime, the differences are small, being greater in the turbulent regime. All these observations can be observed in Figure 10.

It was found that the friction factor, in the adiabatic and diabatic tests, presented a slight difference: *f* is higher for the diabatic case. Andrade [18] also noticed this difference and explains that due to the increase in temperature when there is heat flux, the dynamic viscosity of the fluid, μ, decreases. This explains that the shear stresses on the wall will be lower and thus leading to a reduction in the friction factor, *f*. This effect occurred only in the T5 tube (p=9mm, e=0.4mm) (Figure 10). In the other tubes there is no such decrease in the friction factor, f, when performing the diabatic tests, possibly due to experimental errors such as disturbances due to the equipment used or unevenness of the tubes.

Observing Figure 11, the variation of the pitch causes an increase in heat transfer when the pitch decreases in the turbulent regime. In the laminar regime there are no significant differences. This is since it is a regime where disturbances are attenuated by viscosity and there is no amplification of the mixture in the wall region after corrugation. In the turbulent regime, due to the high Reynolds number, the disturbances are amplified. With the increase of curvature when decreasing the pitch, the

disturbances will be greater, thus increasing the mixture in the smooth area where the wall is circular (after corrugation).

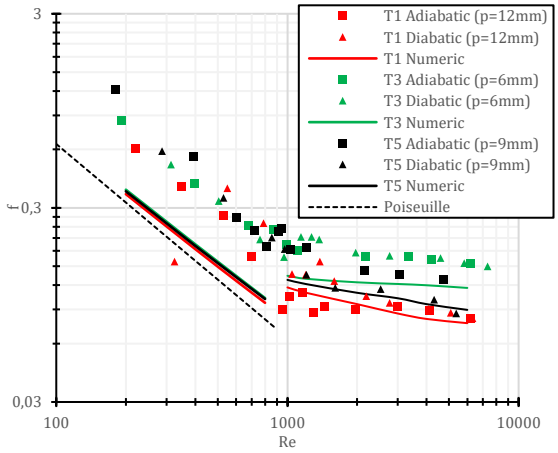

Figure 10 - Influence of the pitch on the friction factor for the same corrugation depth (e=0.4mm). Obtained with a heat flux of 1,9 kW/m^2 − 32,8 kW/m^2.

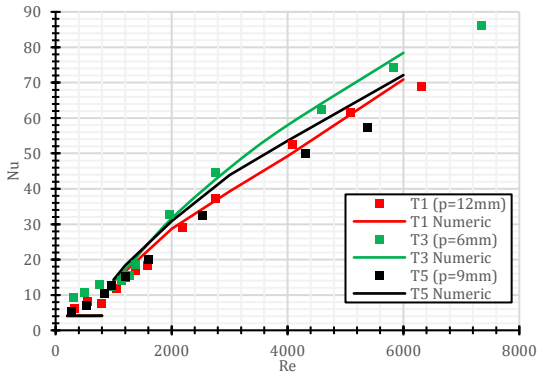

Figure 11 - Points obtained for tubes with different pitches, T1, T3 and T5 (e=0.4mm). Obtained with a heat flux of 1,9 kW/m^2 − 32,8 kW/m^2.

4.4. Effect of depth Variation (T2 vs. T3 and T4 vs. T5)

4.4.1 T2 and T3 comparison

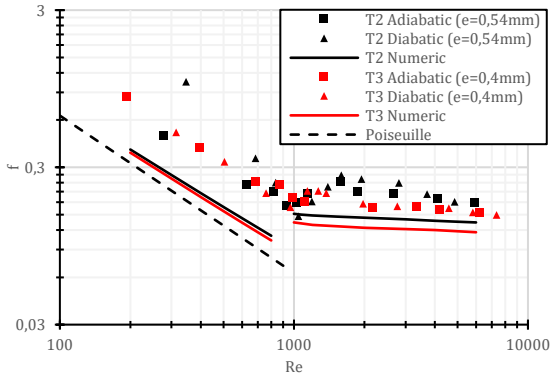

Figure 12 - Comparison of friction factor for different depths, tubes T2 and T3 (p=6mm). Obtained with a heat flux of 2,6 kW/m^2 − 32,8 kW/m^2.

Experimentally, the points obtained with heat transfer (diabatic conditions, with heat flux of 2,6 kW/m^2 − 32,8 kW/m^2) show the behavior described above. Both tests (diabatic and adiabatic) show a clear difference in pressure losses in the turbulent regime being higher for the T2 tube with a depth of 0.54 mm compared to the T3 tube with e=0.4 mm.

Numerically, the results show an increase in the friction factor when the depth of the corrugation is increased both in the laminar regime and in the turbulent flow. The same was verified in the parametric study of the pitch: a small difference in friction losses in the laminar regime and higher in the turbulent regime. The comparations of the results are shown in Figure 12. In this work it was not possible to accurately identify the Reynolds number to which the transition from the laminar to the turbulent regime occurs, when the corrugation depth is changed (e=0.4mm to e=0.54mm). Both Cruz [4] and Vicente *et al.* [5] state that the transition is only a function of dimensional depth of the corrugation. For the tube with lowest depth the transition appears to begin at a Reynolds number close to 1000, while for the other with larger depth it is not possible to identify with certainties where the transition begins.

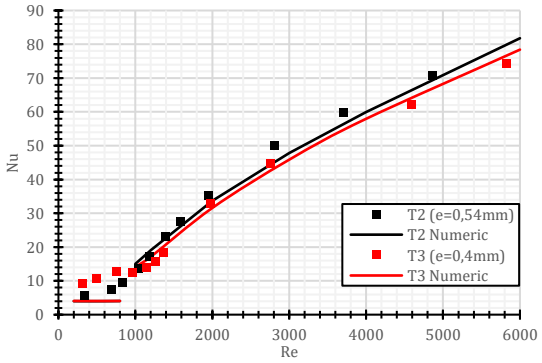

Figure 13 - Representation of Nusselt number for T2 and T3 tubes (p=9mm). Obtained with a heat flux of 2,6 kW/m^2 − 32,8 kW/m^2.

In terms of heat transfer, the Nusselt number is higher for the T2 tube with greater depth, for Reynolds number values greater than 1000, $Re \gtrsim 1000$. This is verified for the experimental and numerical results, thus demonstrating higher heat transfer coefficients for the T2 tube, in the turbulent flow regime. For the laminar regime, the opposite is observed: the heat transfer is higher in the tube with the lowest corrugation depth (T3). The numerical results even show that the T3 tube has a tiny increase in the Nusselt number compared to the T2 tube. However, this part was simulated with fully developed conditions. The same can no longer be guaranteed with the experimental points due to the large increase in the heat transfer coefficient at the beginning of the sections where there is heat flux. That is, there is no guarantee that the flow is developed at the points where the temperatures are

obtained in the laminar regime, that is, the numerical and experimental results are not exactly in the same conditions, in the laminar regime. Figure 13 shows the numerical and experimental points for these tubes.

4.4.2. Comparison between T4 and T5

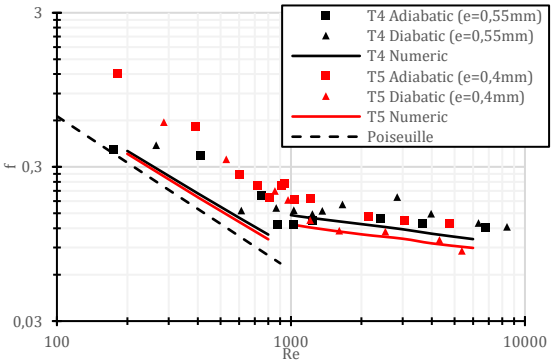

Figure 14 - Comparison of friction factor for different corrugation depths, tubes T4 and T5 (p=9mm). Obtained with a heat flux of 1,9 kW/m^2 − 30,3 kW/m^2.

For these tubes with a 9 mm pitch in the laminar regime, the expected experimental friction factor was inverted. It exhibits a larger friction factor for a tube with lower corrugation depth. This is due to setup errors (joints, unevenness, and pressure sensors). However, the turbulent regime presents an increase in the friction factor, f, when the corrugation depth is increased. This trend agrees with that obtained for the numerical data, obtained for the T2 and T3 tubes, that is, an increase in head losses is observed when the corrugation depth went from 0,4mm to 0,54mm for the tubes with a 6mm pitch. Figure 14 shows the comparison between the two tubes. It was not possible to accurately identify the Reynolds number to which the transition from the laminar to the turbulent flow occurs, as the corrugation depth is changed (e=0.4mm to e=0.54mm). For the tube with greater corrugation depth the transition appears to begin at a Reynolds number close to 900, while for the other with a lesser depth it was not possible to identify with certainties where the transition begins. This corroborates the conclusions of Cruz [4] and Vicente *et al.* [5].

The results obtained for the 9 mm pitch tubes show an increase in the Nusselt number when the corrugation depth is increased. However, the increase is smaller compared to the lower pitch tubes (6 mm) in terms of numerical points. This is probably due to the combined effect of a small pitch and roughly the same difference in the corrugation depth. Since the small pitch tube has greater curvatures, the swirl will have a greater effect on heat transfer and due to this, there is a greater difference for the Nusselt number, for tubes with smaller pitches when changing the depth of the helices. Under experimental conditions and considering that the laminar regime is not thermally fully developed, the T5 tube presents a higher convection heat transfer for Reynolds numbers below 1200, $Re < 1200$. It is thus verified that for Reynolds numbers higher than 1200, the tube with smaller corrugation depth, has a lower capacity to transfer heat. These trends can be observed in Figure 15.

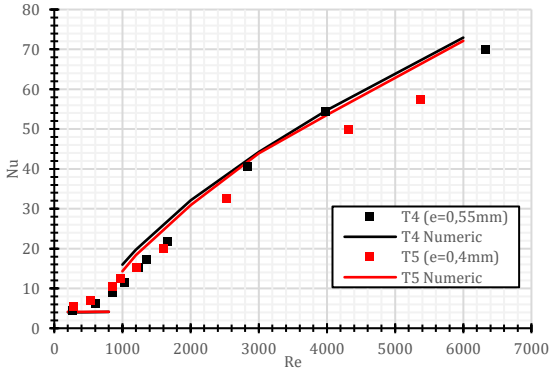

Figure 15 - Nusselt number data for T4 and T5 tubes (p=9mm). Obtained with a heat flux of 1,9 kW/m^2 − 30,3 kW/m^2.

4.5. Differences for f and Nu between tubes

The following figures show the absolute differences between the friction factor and the Nusselt number for each pair of T2-T3 and T4-T5 tubes. It is intended to check which of the pitches (6 or 9 mm) results in larger differences when the corrugation depth is changed.

Observing Figure 16, the differences are greater in the turbulent regime for the T2-T3 tubes in relation to the higher pitch tubes. The larger curvature of the wall to the tubes with 6 mm pitch causes a greater increase in Nusselt number when compared to the 9mm pitch tubes when increasing the depth of the corrugation. This is due to a higher increase in mixing intensity for tubes with lower pitch. However, the tubes with lower pitch have higher friction losses when compared to the 9 mm pitch for the same reasons discussed in the previous paragraphs, when analyzing the effect of changing the corrugation depth.

Figure 17 shows the variation of the friction factor and Nusselt number when the tube pitches are changed to the same depth (e=0.4mm). The greatest differences in pressure losses are verified, as expected for the tubes with the highest pitch difference (T1-T3). Although the head losses between the T1 and T5 tubes have a lower difference, from Reynolds number values greater than 2000, $Re \gtrsim 2000$, the differences between T3 and T5 are greater. This result comes from the reduction of the pitch, which substantially increases the curvature of the walls. The curvature intensifies the secondary swirl movement thus improving the

mixture and increasing disturbances and losses to Reynolds numbers greater than 2000. The pitch reduction from 12mm to 9mm has a smaller curvature increase than the pitch reduction from 9mm to 6mm. For heat transfer, in the laminar regime all pairs of tubes present a neglectful and similar differences when changing the pitch in terms the Nusselt number. This result indicates that the laminar regime does not have benefits, but rather increases in pressure drop. For the turbulent regime it is verified that for Reynolds number values greater than 2000, the largest pitch difference provides the greatest difference between the number of Nusselt since the decrease of the pitch from 12 mm to 6 mm has the maximum increase in the curvature of the walls, having the maximum increase of the fluid mixture enhancing the heat exchange.

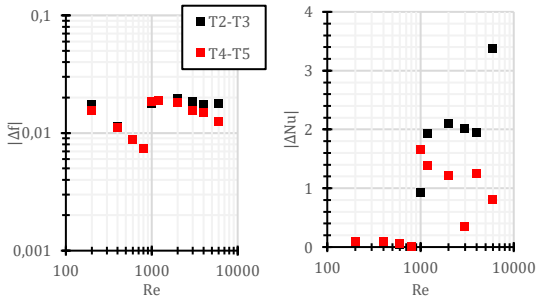

Figure 16 - Differences between f and nu parameters for each pair of tubes T2-T3 (p=6mm) and T4-T5 (p=9mm). T2 (e=0,54mm), T3 (e=0,4mm), T4 (e=0,55mm), T5 (e=0,4mm). Obtained numerically with constant heat flux $\dot{q}'' = 1\ kW/m^2$.

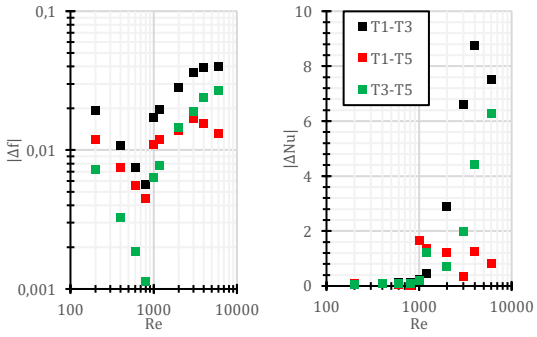

Figure 17 - Parameter differences between tubes with constant depth (e=0,4mm). T1 (p=12mm), T3 (p=6mm), T5 (p=12mm). Obtained numerically with constant heat flux $\dot{q}'' = 1\ kW/m^2$.

4.6. Global comparison

Corrugated tubes always show higher head losses compared to the smooth tube. However, depending on the pitch and depth of the corrugation helices, the friction factor, f, may exhibit different trends. As observed in Figure 18, the friction factor in the laminar regime does not present a great variation in terms of numerical data. But it is possible to distinguish that both the pitch and depth have an influence on the pressure losses. It is observed that the tubes with the lowest pitch and highest corrugation depth (T2) present the highest frictional energy losses for both regimes (laminar and turbulent). T1-type pipes have the lowest pressure losses because they have less accentuated geometry curvatures. It is possible to verify (although the Reynolds number range is not very high) that the pair of tubes T2, T3 and T4, T5 have different variations of f with the Reynolds number i.e., df/dRe between the pairs of tubes. A similar behavior that occurs in smooth tubes is because the relative roughness of the walls influences the friction factor when the number of Reynolds reaches values after the transition ($Re > 3 \times 10^3$). For higher relative roughness, the friction factor takes higher values and presents lower gradients, df/dRe, when compared to tubes with lower relative roughness. This behavior is verified by the Colebrook-White equation, more specifically in the Moody diagram: when relative roughness increases, then in the turbulent regime, the friction factor reaches higher constant values independent of the Reynolds number. Corrugation in a certain way has a behavior like the roughness in smooth tubes.

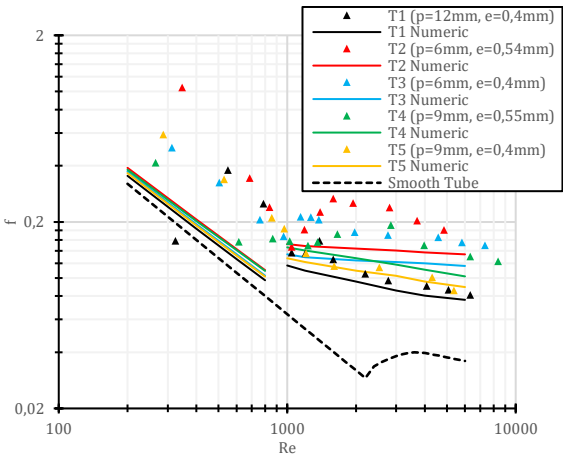

Figure 18 - Global representation of the friction factor of all tubes. Obtained with a heat flux of 1,9 kW/m^2 – 32,8 kW/m^2.

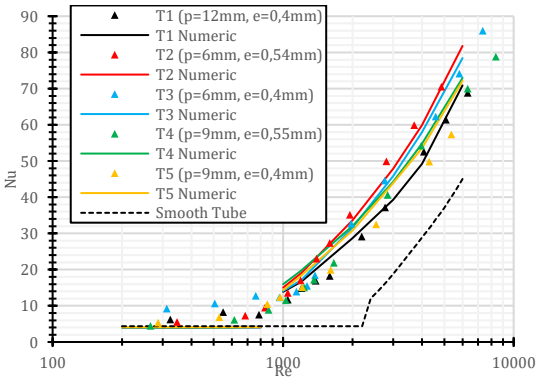

Figure 19 - Global representation of Nusselt number of all tubes. Obtained with a heat flux of 1,9 kW/m^2 – 32,8 kW/m^2.

	Pitch 12 → 9		Depth 0,4 → 0,55		Pitch 9 → 6		Depth 0,4 → 0,54	
T1 $p = 12$ $e = 0,4$	$Nu \uparrow$ $- - \rightarrow$	T5 $p = 9$ $e = 0,4$	$Nu \uparrow$ $- - \rightarrow$	T4 $p = 9$ $e = 0,55$	$Nu \uparrow$ $- - \rightarrow$	T3 $p = 6$ $e = 0,4$	$Nu \uparrow$ $- - \rightarrow$	T2 $p = 6$ $e = 0,54$
					Depth 0,55 → 0,4			

Figure 20 - Qualitative evolution of the Nusselt number to a Reynolds number above 3000 when changing geometry.

	Pitch 12 → 9		Depth 0,4 → 0,55		Pitch 9 → 6		Depth 0,4 → 0,54	
T1 $p = 12$ $e = 0,4$	$f \uparrow$ $- - \rightarrow$	T5 $p = 9$ $e = 0,4$	$f \uparrow$ $- - \rightarrow$	T4 $p = 9$ $e = 0,55$	$f \uparrow$ $- - \rightarrow$	T3 $p = 6$ $e = 0,4$	$f \uparrow$ $- - \rightarrow$	T2 $p = 6$ $e = 0,54$
					Depth 0,55 → 0,4			

Figure 21 - Qualitative evolution of the friction factor to a Reynolds number above 3000 when changing geometry.

The results for the Nusselt number for all tubes are shown in Figure 19. Figure 20 describes how geometry varies so that the Nusselt number has a growth for $Re > 3000$. This growth is due once again to the growth of the curvatures of the walls as the geometry changes, according to Figure 20, intensifying the swirl movement and mixing. These increases also have the same effect for friction factor f, as disturbances and losses increase. Figure 21 schematizes the previous sentence. In the laminar regime there are no improvements when changing the geometry, probably due to the disturbances and mixing being very weak or non-existent in this regime.

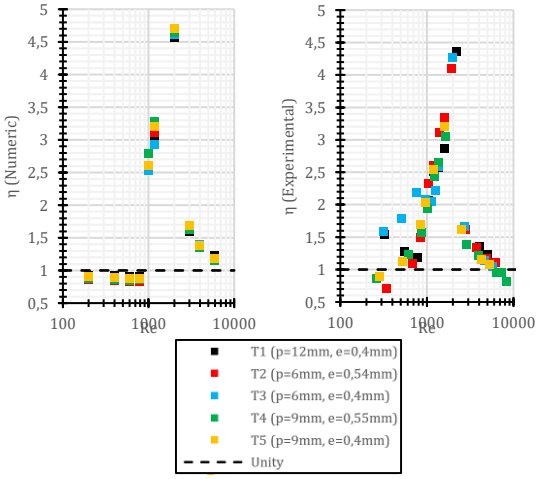

Figure 22 - Thermal performance of the points obtained numerically and experimentally for all tubes. Obtained with a heat flux of 1,9 $kW/m^2 - 32,8\ kW/m^2$.

However, for the thermal performance, η, it is verified that the tubes have greater efficiency for the transition regime ($1000 < Re_D < 2000$). For Reynolds number values between 1000 and 4000, 9mm pitch tubes (T4 and T5) perform better than all other tubes. These results are consistent with the analysis of head losses and heat transfer performed in the previous sections. For Reynolds number values greater than 4000 the T1 (lowest wall curvature) tube has the best performance although at this regime the thermal performance is lower compared to the transition regime since the pressure losses will be the lowest compared to the other tubes keeping the heat transfers high. Thus, the thermal performance, η, although lower than in the transition regime, will be higher than that of the other tubes. For the laminar regime, the corrugation does not present improvements in performance. The experimental data have a good agreement with the previous one, except for the laminar regime. This is since the flow is once again not fully thermally developed.

5. Conclusion

This work was carried out following the study developed by Cruz [4] with the objective of studying the influence of corrugated tube geometry on their performance, heat transfer and friction losses. Five tubes with different corrugation depths and pitches were provided for further completion of this study. The work was developed complementing the experimental work with a numerical approach.

With the numerical model introduced in the Star-CCM+ 2019 program [13], all tubes were simulated by doing a study in terms of polyhedric mesh convergence and the points and curves for each tube were obtained. The $k - \omega$ SST (Menter) turbulence model was used to model the turbulent regime.

To validate the numerical results, the tubes were tested on an experimental setup where fundamental data can be acquired for the calculation of the parameters of interest. The experimental bench has been validated in previous studies. The numerical results showed good agreement with the experimental ones, which allowed the validation of the computational model. Analyzing the data, it is verified that the transition from laminar to turbulent regime begins at a Reynolds number of 1000 for tubes with lower corrugation depth, while tubes with the highest depth depict a critical Reynolds number value to start the transition from laminar to turbulent regime close to 900. In addition, the pitch is the geometric parameter that most influences heat exchange in this work. The corrugation depth substantially increases head losses when compared to the pitch. The depth variation presents a smaller increase in the Nusselt number. In terms of thermal performance, the corrugated tubes do not present better performances in the laminar regime (numerically) compared to the smooth tube. All tubes have a maximum performance for a range of Reynolds numbers of 1000<Re<2000, i.e., in the

transition region. The 9mm pitch tubes (T4 and T5) have the best performance for a range of Reynolds numbers between 1000 and 4000.

Referências

[1] Z. S. Kareem, M. M. Jaafar, T. M. Lazim, S. Abdullah e A. F. Abdulwahid, "Passive heat transfer enhancement review in corrugation," *Experimental Thermal and Fluid Science,* pp. 22-38, Novembro 2015.

[2] A. García, J. P. Solano, P. G. Vicente e A. Viedma, "The influence of artificial roughness shape on heat transfer enhancement: Corrugated tubes, dimpled tubes and wire coils," *Applied Thermal Engineering,* pp. 196-201, Março 2012.

[3] F. Andrade, A. S. Moita, A. Nikulin, A. Moreira e H. Santos, "Experimental investigation on heat transfer and pressure drop of internal flow in corrugated tubes," *International Journal of Heat and Mass Transfer,* pp. 940-955, Setembro 2019.

[4] G. J. Cruz, "Experimental and numerical characterization of the flow and heat transfer inside corrugated pipes," *Dissertação para a obtenção do Grau de Mestre em Engenharia Mecânica,* 2019.

[5] P. G. Vicente, A. García e A. Viedma, "Mixed convection heat transfer and isothermal pressure drop in corrugated tubes for laminar and transition flow," *International Communications in Heat and Mass Transfer,* pp. 651-662, Julho 2004.

[6] P. G. Vicente, A. García e A. Viedma, "Experimental investigation on heat transfer and frictional characteristics of spirally corrugated tubes in turbulent flow at different Prandtl numbers," *International Journal of Heat and Mass Transfer,* pp. 671-681, Agosto 2003.

[7] J. I. Córcoles-Tendero, J. F. Belmonte, A. E. Molina e J. A. Almendros-Ibáñez, "Numerical simulation of the heat transfer process in a corrugated tube," *International Journal of Thermal Sciences,* pp. 125-136, Abril 2018.

[8] W. Wang, Y. Zhang, Y. Li, H. Han e B. Li, "Numerical study on fully-developed turbulent flow and heat transfer in inward corrugated tubes with double-objective optimization," *International Journal of Heat and Mass Transfer,* pp. 782-792, 2017.

[9] Z.-j. Jin, F.-q. Chen, Z.-x. Gao, X.-f. Gao e J.-y. Qian, "Effects of pitch and corrugation depth on heat transfer characteristics in six-start spirally corrugated tube," *International Journal of Heat and Mass Transfer,* pp. 1011-1025, Dezembro 2016.

[10] S. Pethkool, S. Eiamsa-ard, S. Kwankaomeng e P. Promvonge, "Turbulent heat transfer enhancement in a heat exchanger using helically corrugated tube," *International Communications in Heat and Mass Transfer,* pp. 340-347, 5 Dezembro 2010.

[11] ASM Aerospace Specification Metals, Inc., "ASM Material Data Sheet," [Online]. Available: http://asm.matweb.com/search/SpecificMaterial.asp?bassnum=MQ304A. [Acedido em 14 Novembro 2020].

[12] Autodesk, Inc., "AutoCAD para Mac e Windows," [Online]. Available: https://www.autodesk.pt/products/autocad/overview?plc=ACDIST&term=1-YEAR&support=ADVANCED&quantity=1.

[13] Siemens, "Star-CCM+," [Online]. Available: https://www.plm.automation.siemens.com/global/pt/products/simcenter/STAR-CCM.html.

[14] Q.-H. Deng e G.-F. Tang, "Special treatment of pressure correction based on continuity conservation in a pressure-based algorithm," *Numerical Heat Transfer, Part B: Fundamentals,* pp. 73-92, 30 Novembro 2010.

[15] R. G. Sargent, "Verification and validation of simulation models," *Proceedings of the 2010 Winter Simulation Conference,* 6 Janeiro 2011.

[16] F. A. Ferreira, "Construção e teste de uma instalação experimental para estudo dos mecanismos de transmissão de calor em escoamentos com convecção forçada - aplicação a sistemas de recuperação de energia térmica em veículos," *Dissertação para a obtenção do Grau de Mestre em Engenharia Mecânica,* Julho 2016.

[17] A. Nikulin, A. S. Moita, S. Murshed, A. Huminic, Y. Grosu, A. Faik, J. Nieto-Maestre e O. Khliyeva, "Effect of Al2O3 nanoparticles on laminar, transient and turbulent flow of isopropyl alcohol," *International Journal of Heat and Mass Transfer,* p. 1032–1044, Outubro 2018.

[18] F. A. Andrade, "Caracterização Experimental da Transmissão de Calor em Escoamentos no Interior de Tubos Corrugados," *Dissertação para a obtenção do Grau de Mestre em Engenharia Mecânica,* 2018.

[19] B. N. Taylor e C. E. Kuyatt, Guidelines for Evaluating and Expressing the Uncertainty of NIST Measurement Results, 1994.

[20] J. R. Taylor, Introduction to Error Analysis, Cailfornia: University Science Books, 1997.